UCRL-JC-129810
PREPRINT

High Pressure Solid State Experiments on the Nova Laser

D.H. Kalantar, B.A. Remington, E.A. Chandler, J.D. Colvin, D.M. Gold, K.O. Mikaelian,
S.V. Weber, L.G. Wiley - LLNL
J.S. Wark - University of Oxford
A.A. Hauer - Los Alamos National Laboratory
M.A. Meyers - University of California San Diego

This paper was prepared for submittal to the
1998 Hypervelocity Impact Symposium (HVIS)
Huntsville, AL
November 16 - 19, 1998

11/98

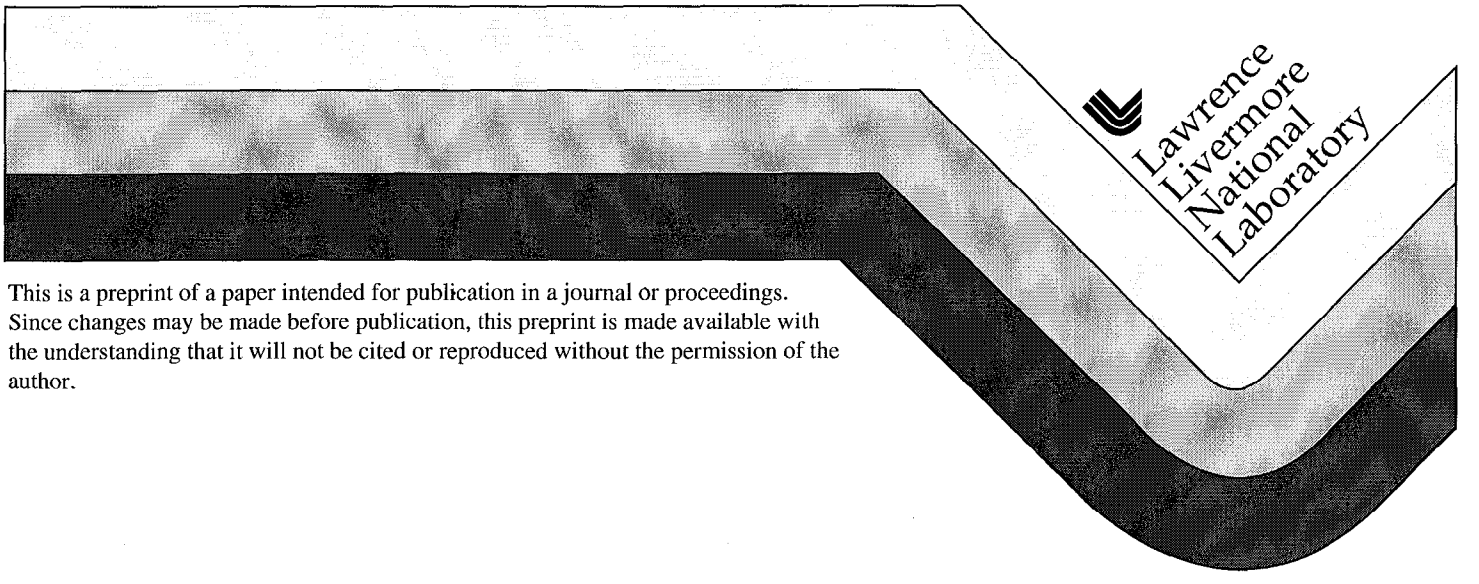

Disclaimer:

HIGH PRESSURE SOLID STATE EXPERIMENTS ON THE NOVA LASER

D. H. KALANTAR*, B. A. REMINGTON*, E. A. CHANDLER*, J. D. COLVIN*, D. M. GOLD*, K. O. MIKAELIAN*, S. V. WEBER*, L. G. WILEY*, J. S. WARK, A. A. HAUER***, M. A. MEYERS******

*Lawrence Livermore National Laboratory, Livermore, CA 94550; *Department of Physics, Clarendon Laboratoy, University of Oxford, Oxford, UK OX1 3PU; *** Los Alamos National Laboratory, Los Alamos, NM 87545; ****University of California at San Diego, La Jolla, CA 92043

Summary — An x-ray drive has been developed to shock compress metal foils in the solid state in order to study the material strength under high compression. The drive has been characterized and hydrodynamics experiments designed to study growth of the Rayleigh-Taylor (RT) instability in Cu foils at 3 Mbar peak pressures have been started. Pre-imposed modulations with an initial wavelength of 20-50 μm, and amplitudes of 1.0-2.5 μm show growth consistent with simulations. In this parameter regime, the fluid and solid states are expected to behave similarly for Cu. An analytic stability analysis is used to motivate an experimental design with an Al foil where the effects of material strength on the RT growth are significantly enhanced. Improved x-ray drive design will allow the material to stay solid under compression throughout the experiment, and dynamic diffraction techniques are being developed to verify the compressed state.

INTRODUCTION

In a classical fluid model, when a light fluid accelerates a heavier fluid, the interface is Rayleigh-Taylor (RT) unstable. As a result, any mass modulation at the embedded material interface is unstable, and can grow when accelerated. However, when the material is in the solid state, the strength of the material can counter the effect of the RT instability. The parameters that define whether a material is stable or unstable to instability growth in the solid state depend on the wavelength and amplitude of the modulation, the acceleration, foil thickness, and material properties, such as yield stress, shear modulus, and the acceleration history.

Solid state instability growth will occur in the plastic flow regime. Plastic behavior is described by a semi-empirical constitutive model [1] that has been developed for phenomena that occur at strain rates $<10^5$ s^{-1}. Such plastic flow has been characterized either microscopically by the theory of lattice dislocations, or macroscopically by an effective lattice viscosity [2]. The best approach to describe the plastic flow of a material may depend on the specifics of the particular experiment. Neither approach has been well tested experimentally.

Analytically, stability boundaries can be defined, as described by Lebedev *et al* [3, 4], which can be used to determine whether material strength is sufficient to inhibit plastic deformation, completely stabilizing growth of a modulation. Outside the stability boundary, the material may undergo plastic deformation, and the modulated interface may grow. This has been demonstrated by Barnes *et al* [5] using Al plates with a preimposed surface modulation that are driven with a high explosive drive, and also by Lebedev *et al*, [3, 4] using Al and Ti plates in similar experiments.

We are conducting experiments on the Nova laser [6] to study the plastic flow of metals at high pressure and very high strain rates. Metal foils of copper are compressed by a factor of 1.5-2.0 with staged shocks reaching peak pressures of about 3 Mbar. The Rayleigh-Taylor instability is the observable "probe" in this experiment, with departures from classical (liquid) behavior characterizing the material strength properties at high pressure and compression.

We present details in this paper of the hohlraum target design and x-ray drive characterization for a Cu foil experiment. We also present calculations of the material state with this drive, and results from instability growth experiments using thin Cu foils. We discuss the stability boundaries for solid state plastic flow for the Nova experiments, and conclude with a discussion of an improved experimental design using an Al foil where the foil remains solid throughout the experiment and strength effects should be considerably enhanced.

EXPERIMENTAL DETAILS

The hydrodynamics experiments are conducted using an x-ray drive created in a cylindrical gold hohlraum. This x-ray drive accelerates a metal foil payload by ablation of a brominated polystyrene ablator layer. A preimposed sinusoidal modulation is located on the metal foil at the embedded interface. The growth of this R-T unstable interface is then diagnosed by face-on x-ray radiography using a gated x-ray framing camera. [7]

The target geometry is shown in Fig. 1. The hohlraum (Fig. 1a) is cylindrically symmetric with internal shielding to prevent hard x-rays from preheating the Cu foil due to M-band emission coming from the laser spots on the inner hohlraum wall. The hohlraum is 3.44 mm in diameter, and 5.75 mm long. The laser entrance holes are 1.2 mm in diameter, and the holes in the internal shields are 1.6 mm in diameter.

The hydrodynamics package (Fig. 1b), consisting of a 20 μm thick brominated polystyrene (CH(Br)) foil pressed in contact with the metal foil, is mounted on the side of the hohlraum. The CH(Br) ablator has a 3% atomic Br fraction to enhance the opacity to the soft x-rays. We typically use 18-19 μm thick oxygen-free high conductivity Cu foils that have been rolled and then machined to have a sinusoidal amplitude modulation.

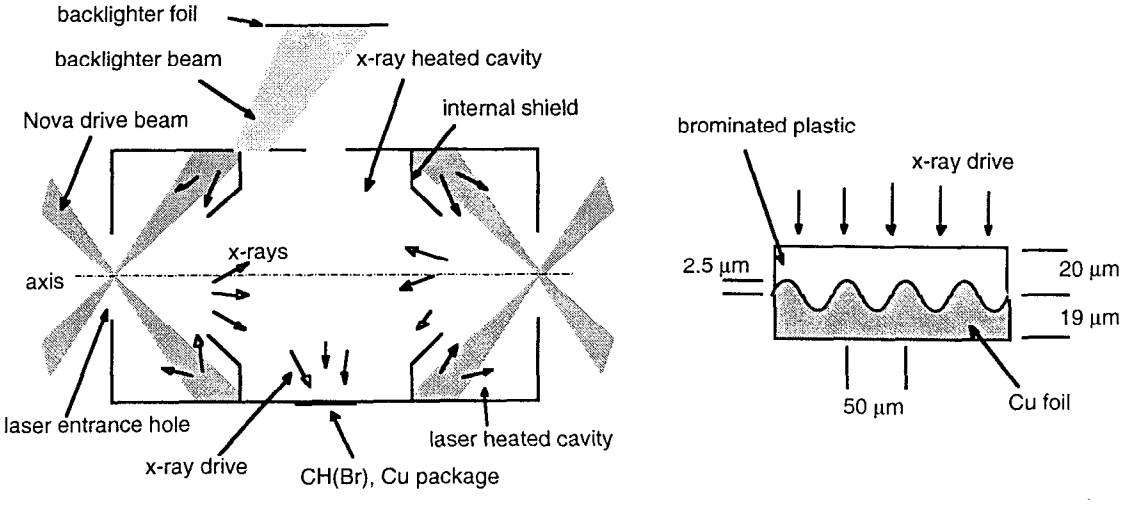

a) Hohlraum target b) Rayleigh-Taylor package

Fig. 1: (a) Schematic showing the internally shielded hohlraum and geometry for face-on radiography. (b) Moduldated foil package mounted on the side of the hohlraum.

Eight Nova beams generate an x-ray radiation environment in the two laser heated cavities of the target. Re-emitted x-rays that pass through the holes in the internal shields heat the central (x-ray heated) cavity and ablate material from the CH(Br) ablator, launching a series of shocks into the package. Without the internal shields, the 2-4 keV Au M-band component of the spectrum of emission from the laser plasmas would be absorbed throughout the full volume of the package, potentially preheating the Cu foil causing it to melt and decompress. With the internal shielding, the x-rays incident on the ablator are generated by re-emission from the regions of the wall that are not directly illuminated by the laser beams, and the spectrum of these x-rays is nearly Planckian without a significant M-band component.

The x-ray drive ablates the brominated plastic, launching a series of shocks into the metal foil, compressing and accelerating it away from the hohlraum. We diagnose the growth of the perturbed unstable embedded interface by x-ray radiography using a large area (0.7 mm diameter focal spot) backlighter generated with two additional Nova beams aligned to a separate Fe backlighter foil generating He_α x-rays at 6.7 keV. A 2-3 ns square laser pulse shape was used for these backlighter beams, and delays relative to the drive beams ranged from 5-14 ns.

X-RAY DRIVE MEASUREMENT

The laser pulse shape is designed to generate an x-ray drive to launch 2 shocks, compressing the Cu foil to a peak pressure of about 3 Mbar while maintaining the metal foil in the solid state. This pulse shape is shown in Fig. 2. It has an intensity ratio in the peak vs. the foot of about 30. We have characterized the x-ray drive using the Dante diagnostic [8] and side on foil trajectories.

The Dante diagnostic is a filtered array of absolutely characterized x-ray diodes. These are positioned to view the spectral soft x-ray emission from the inner wall of the central section of the hohlraum through a beryllium-lined diagnostic hole. With the high contrast shaped laser pulse, only the lowest energy channels of the Dante detected signals starting at about 1.0 ns. The absolute signal levels from these diodes were used to estimate the Planckian drive temperature, which started at about 15 eV and rose to 40 eV at 3.5 ns. Above 40 eV, enough channels recorded signals that a spectral unfold could be performed. The measured radiation temperature rose from 40 eV at 4.0 ns to 90 eV at the end of the laser pulse at 6.5 ns, and then slowly decayed as energy was lost into the hohlraum walls and through the laser entrance holes.

The measured drive temperature is shown overlaid with the laser pulse shape in Fig. 2. Note that the measured drive is the re-emission from the wall of the hohlraum at the midplane. The package experiences the x-ray drive that is incident on the wall, the incident flux temperature (T_I),

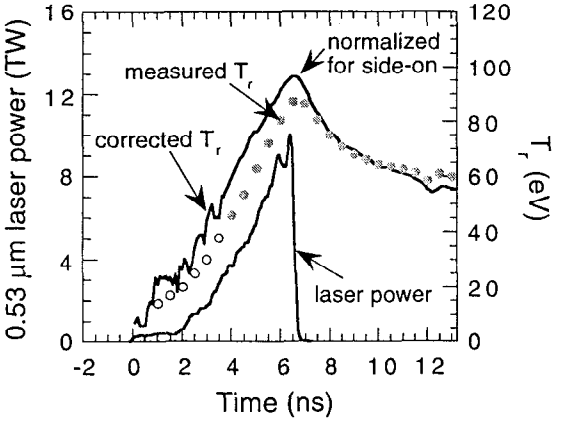

Fig. 2: Laser pulse shape and x-ray drive temperature for the low isentrope drive.

which is related to the measured re-emission flux temperature (T_R) by the albedo (α) [9] of the wall by the equation:

$$T_I = T_R/\alpha^{1/4} \tag{1}$$

We calculated the albedo correction using the LASNEX computer code [10], incorporating a view-factor analysis where the flux incident on the wall at the midplane of the target is calculated from the view of the different regions of the hohlraum. We also performed a full simulation of the hohlraum target including the laser power incident in the laser heated regions to estimate the drive temperature at the package. The resulting corrected drive is shown overlaid in Fig. 2. As a consistency check for the low temperature foot portion of the pulse, we analytically solve the power balance prescription from Rosen and Lindl [11]. We consider the power flow in the laser heated and x-ray heated cavities of the internally shielded hohlraum. The laser power that enters the laser heated cavities is equal to the sum of the losses through the laser entrance hole, losses into the wall, and power flow into the x-ray heated cavity. Similarly, the power flow into the x-ray heated cavity is equal to losses to the hohlraum wall and losses out to the laser heated cavities. Incorporating the temporal scaling of the wall albedo from high power 1 ns drive experiments, we estimate that the temperature of the foot at 1 ns is about 24 eV. The LASNEX albedo corrected drive is in good agreement with this scaling at 20-25 eV.

The peak portion of the drive is verified with a side-on foil trajectory measurement. For this, we mounted a package consisting of 22 μm CH(Br) with 13 μm Cu on the side of the hohlraum. We recorded an x-ray shadow image of the foil as it was accelerated away from the hohlraum using a high magnification (55X) x-ray streaked imager. In order to match the overall motion of the foil, the albedo corrected drive is reduced in the simulations by only about 2% in radiation temperature, T_R, for times t>5 ns. This adjustment is interpreted as a correction due to the uncertainty in the opacity of the ablator at low drive temperatures, and in the initial Dante drive measurement itself.

Using the albedo corrected x-ray drive in the hohlraum, we model the conditions in the foil package with 1-D LASNEX. The calculated temperature and pressure at the embedded ablator/Cu interface are shown in Fig. 3. The x-ray drive ablatively launches two shocks into the copper. The first shock due to the low foot is about 0.4 Mbar in the Cu, and the second is 3 Mbar. There are subsequent reflected shocks that maintain the high pressure until about 8 ns. At about this time, the material temperature at the interface exceeds the melt temperature, which we calculate by the Lindemann law:

$$T_m = T_{mo} exp\{2a(1-1/\eta)\}\eta^{2(\gamma_o - a - 1/3)} \tag{2}$$

where T_{mo} is the melt temperature at constant volume, η is the compression of the sample, γ is the Grüneisen gamma, and a is the coefficient of volume dependence of γ, as defined by Steinberg *et al* [1].

The low isentrope drive is calculated to keep the foil very near an adiabat throughout the experiment. In Fig. 4 we show the internal energy at the Cu interface plotted as a function of density (compression) from t=0 to t=15 ns. Note that this trajectory is sensitive to the temperature of the foot of the shaped drive pulse. If the albedo correction for the foot is incorrect, the timing of the first shock may be off. In particular, if the foot drive is much lower then the second shock may catch up before it reaches the interface, placing the metal foil on a higher adiabat and potentially melting it. For the case of this drive, the shocks overlap about half way through the foil, melting the back side. The interface then melts with the rarefaction.

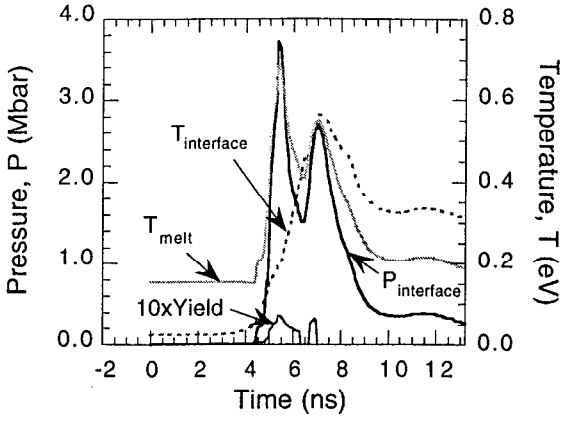

Fig. 3: Pressure and temperature calculated at the CH(Br)/Cu interface with the low isentrope drive.

Adjusting the level of the foot somewhat higher is one way to keep the temperature at the interface below the melt curve for longer, as is discussed later.

Experiments to characterize the foot drive were done using both active shock breakout [12, 13] and dynamic Bragg diffraction techniques [14, 15] to measure shock timing. For the case of the active shock breakout measurement, we use a displacement Michaelson interferometer to measure motion of the back surface of a 17 μm thick Al flat target mounted on the side of the hohlraum. Motion of the back surface due to the shock transit and breakout through the foil is evident by a shift in the fringe pattern, as shown in Fig. 5. The streaked interferometer data is shown in Fig. 5a, and the analyzed position as a function of time for the back surface is shown in Fig. 5b. This measurement is done with an interferometer that operates at a wavelength of 400 nm, so a full fringe shift corresponds to one half wavelength (0.2 μm) of motion at the back surface.

The interferometer data shows motion that may be due to the breakout of the elastic precursor wave or due to some amount of preheat at the back surface of the Al foil, and then the rapid motion and disappearance of the fringes as the main shock breaks out. We show simulated position as a function of time for the back surface with some imposed preheat to illustrate how this measurement is affected by low preheat levels.

For the case of Bragg diffraction, we use a CH(Br) ablator with a 40 μm thick Si crystal as a

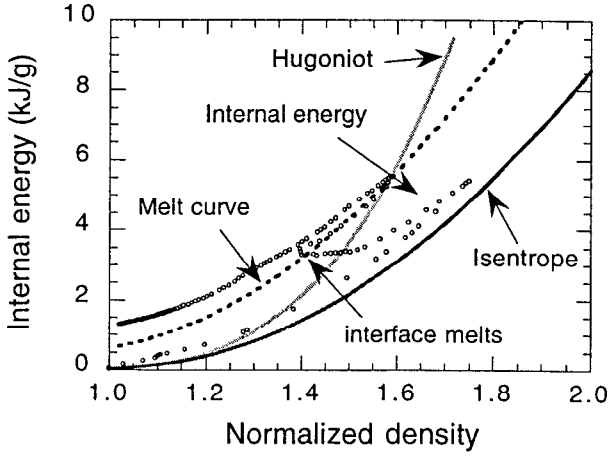

Fig. 4: Internal energy trajectory of the Cu at the CH(Br)/Cu interface for the low isentrope x-ray drive.

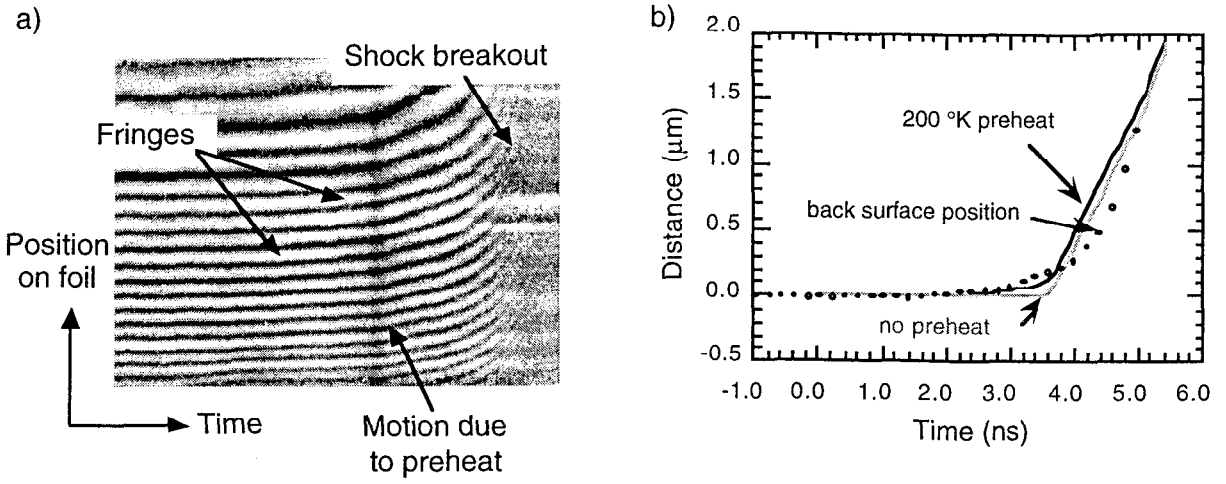

Fig. 5: Displacement interferometer data showing the motion of the back surface of a 17 μm Al foil due to the shaped laser drive. Streak data showing the fringes is shown in (a). Reduced data is shown with simulation in (b).

surrogate for the Cu foil mounted on the side of the hohlraum. A vanadium backlighter generates x-rays at 5.3 keV, diffracting off the crystal through the brominated plastic ablator. When the shock transits the ablator and reaches the interface, it compresses the Si lattice. This is observed as a shift in the Bragg diffraction angle of the backlighter x-rays. Data obtained using this technique with a square laser pulse shape is shown in Fig. 6 to illustrate the technique. [14-16] The estimated shock strength in the Si for this experiment was 350 kbar, compared to the calculated 650 kbar first shock strength in Cu for this shaped x-ray drive. Note that the presence of the diffraction signal under shock compression is consistent with the assumption that the Si remains solid under compression.

INSTABILITY GROWTH EXPERIMENTS

Sinusoidal modulations are machined in the Cu foils with amplitudes of 1.0-2.5 μm, and wavelengths of 20 and 50 μm. A 20 μm thickness of brominated plastic ablator is pressed onto the modulated foils, and then the package is mounted over a hole in the side of the hohlraum. The x-ray drive ablatively launches a series of shocks to compress and accelerate the metal foil away from the side of the hohlraum.

Radiographic images of the foil are recorded using 6.7 keV Fe x-rays. Up to 16 images are recorded on 4 independently timed microchannel plate striplines on each laser shot, using the Flexible X-ray Imager [17] with a 230 ps gate pulse. The modulation amplitude in optical depth is calculated by Fourier analysis at each time. The Fourier amplitude is normalized to the initial contrast in optical depth, which we measured on a separate shot.

The growth factors for λ=50 μm, 2.5 μm amplitude modulations are shown in Fig. 7a, and for λ=20 μm, 1.0 μm amplitude modulations are shown plotted in Fig. 7b. In these experiments, the ablator/metal interface moves only about 40 μm during the time the measurements are made and the overall growth factors are small, which means the modulation remains nearly linear. As a result, when we normalize the measurements with the initial (measured) contrast at that wavelength (x-ray mean free-path and instrument resolution function), the instrument resolution (MTF~0.65 at 8X instrument magnification for λ=50 μm and 0.6 at 12X for λ=20 μm) is removed from the measurement.

Overlaid on the graphs in Fig. 7, we have plotted the growth factors simulated with LASNEX using both a fluid model, and the constitutive material strength model described by Steinberg *et al.*

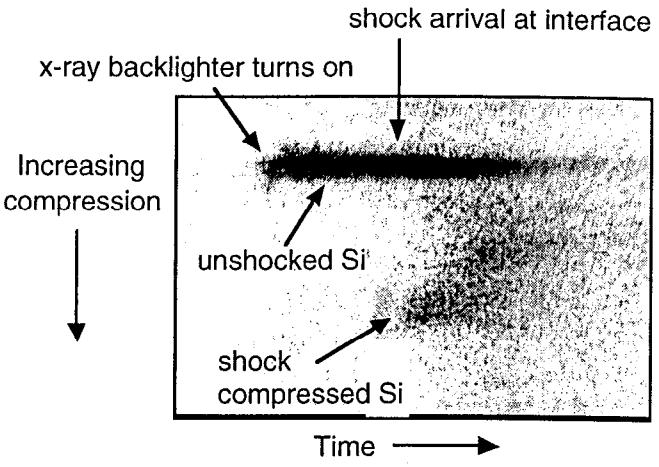

Fig. 6: Streaked diffraction pattern from the CH(Br)/Si embedded interface showing a shift in the diffraction peak at the time the shock reaches the interface.

We show separate calculations in Fig. 7 for experiments where the peak portion of the laser pulse shape was reduced by about 20% (indicated on the figure by 'low drive') since the growth is sensitive to the actual drive history. The difference between the fluid and material strength simulations for λ=20 μm and 50 μm is small. For the 50 μm wavelength case, the simulations are nearly identical. For the 20 μm wavelength case, material strength leads to about 20% less growth, but the difference due to variation in the laser power history for the different shots is about this order, making it difficult to confirm that reduced growth is due to the material strength at $\lambda \geq 20$ μm with these Cu foils.

Extending the simulations to shorter modulation wavelengths, $\lambda < 20$ μm, we observe a greater effect due to material strength. The calculated growth factors for a range of wavelengths from 5 to 50 μm are shown in Fig. 8, plotted after the interface has moved a distance of 20 μm. The enhanced difference between fluid and strength modeling at $\lambda \leq 20$ μm suggests that with some modifications we should be able to observe the effect of strength stabilization in the Nova experiments. Measuring perturbation growth factors at λ=5-10 μm with gated pinhole imaging is problematic due to reduced exposure levels and diffraction effects with apertures smaller than 5 μm. As a result, this experiment would be improved with a design where longer wavelengths would be stabilized.

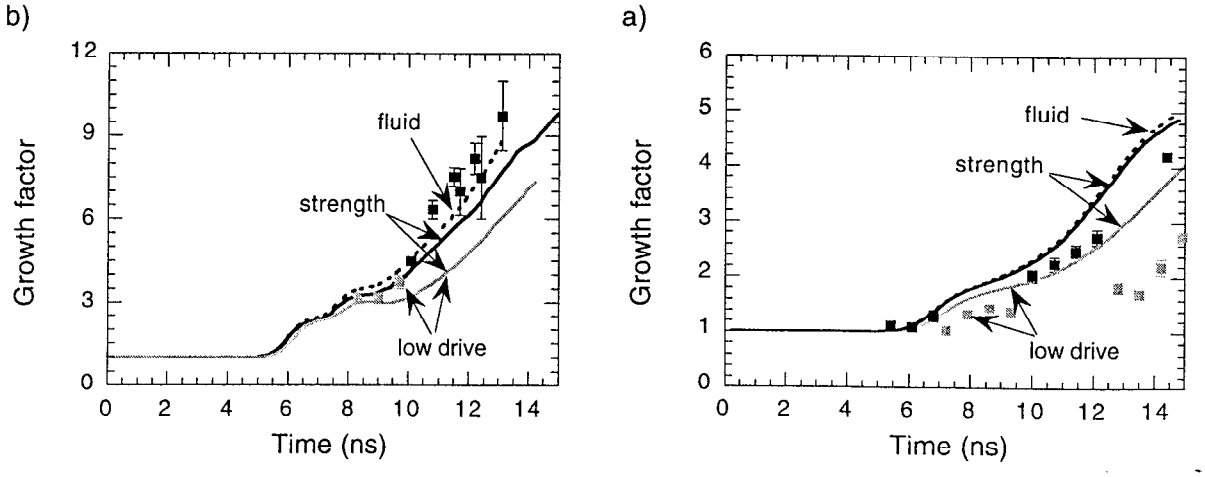

Fig. 7: Instability growth factors for a) 50 μm and b) 20 μm wavelength modulation at the embedded CH(Br)/Cu interface. LASNEX simulations were done with and without strength.

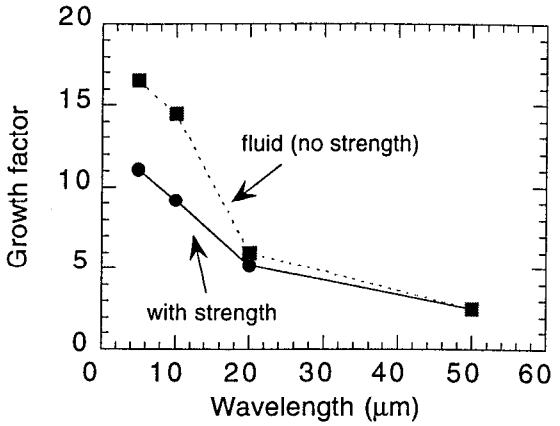

Fig. 8: Growth factor as a function of wavelength for a modulated Cu foil, plotted for a distance moved of 20 μm.

STRENGTH STABILIZATION

The pressure enhanced yield strength and shear modulus are given in the strain-rate independent constitutive model by Steinberg *et al* as

$$Y(P,T) = Y_o\left[1+\beta(\varepsilon+\varepsilon_i)\right]^n\left[1+\left(\frac{Y_P'}{Y_o}\right)\frac{P}{\eta^{1/3}}-\left(\frac{G_T'}{G_o}\right)(T-300)\right] \tag{3a}$$

$$G(P,T) = G_o\left[1+\left(\frac{G_P'}{G_o}\right)\frac{P}{\eta^{1/3}}-\left(\frac{G_T'}{G_o}\right)(T-300)\right] \tag{3b}$$

where the Y is the yield strength, and G is the shear modulus, ε is the strain, and η is the compression. In this formulation, the pressure (P) and temperature (T) dependence and the effect of work hardening (β) are included. The initial value for yield strength is Y_o=1.2x10^{-3} Mbar and the initial value for shear modulus is G_o=0.477 Mbar for a Cu foil.

At a shock pressure of 3 Mbar, the Cu foil is compressed by about a factor of >1.5, at which point the yield strength is 50 kbar, enhanced by a factor of about 40 over the nominal value, Y_o. The shear modulus is about 3.6 Mbar. Under these conditions, the yield strength is exceeded by more than an order of magnitude, putting the foil into the plastic flow regime and allowing for instability growth in the solid state.

Estimates can be made as to whether the modulation on the Cu package grows or not, based on a stability boundary analysis assuming steady-state conditions. The Miles criterion, based on linear theory, [18] assumes a modulation amplitude, η_o, much smaller than the wavelength. It establishes that for a semi-infinite slab with a modulated surface, the modulation is stable if its wavelength is shorter than the cutoff wavelength,

$$\lambda_\infty = 4\pi G \Big/ \rho g \tag{4}$$

where g is the acceleration. Including the finite thickness of the foil, Lebedev *et al* extend Miles' theory and predict this cutoff is at

$$\lambda_c = \frac{2\lambda_\infty}{1+\sqrt{1+8\sqrt{3}c^2/gH}} \tag{5}$$

where c is the speed of the shear wave, and λ_∞ corresponds to the Miles cutoff wavelength, Eqn. (4). For the conditions of this experiment, λ_c=30 μm. Therefore, at λ=20 μm, we are below the cutoff wavelength, suggesting that perturbations with very small initial amplitude under steady state conditions should not grow.

We observe, however, the λ=20 μm modulation grows in both the experiment and the simulation. This is because the amplitude exceeds the critical amplitude given by Lebedev *et al.* This amplitude cutoff is given by the expression:

$$\eta_c = \eta_c(Drucker)\left[1-0.86e^{(2\pi H/\sqrt{3}\lambda)}\right]\left\{\left[1-e^{(-2\pi H/\sqrt{3}\lambda)}\right]^2-\left(\frac{\lambda}{\lambda_\infty}\right)^2\right\} \tag{6}$$

where

$$\eta_c(\text{Drucker}) = \frac{2Y}{\rho g} \tag{7}$$

is the wavelength independent critical amplitude threshold to instability growth from Drucker [19]. For these experiments, at λ=20 μm, the amplitude threshold is <1 μm, which is much too small to diagnose by x-ray backlighting using a hard x-ray backlighter at 6.7 keV.

In order to design an experiment in a regime where there is a much greater reduction in growth due to material strength, we consider a material with a lower density and a larger value for the derivative of the yield strength with pressure to maximize the effect of strength on the R-T instability growth. Aluminum is one such metal with a pressure derivative of the yield strength that is a factor of 2 larger than for Cu. For 7075 (or 6061) Al, which has an initial yield strength of 4.2 kbar, we calculate the growth of 20 μm wavelength with and without strength using an initial amplitude of 0.5 μm. The case with strength grows less than a factor of 2 while the fluid case shows a growth factor of about 5 at t=12 ns (Fig. 9a). Note that in order to time the shocks so that they do not overlap in the metal foil, the foot portion of the drive is raised (Fig. 9b). With this design, the peak pressure in the Al is 1.4 Mbar, and the foil is calculated to remain solid throughout, as indicated by a plot of the internal energy trajectory (Fig. 10).

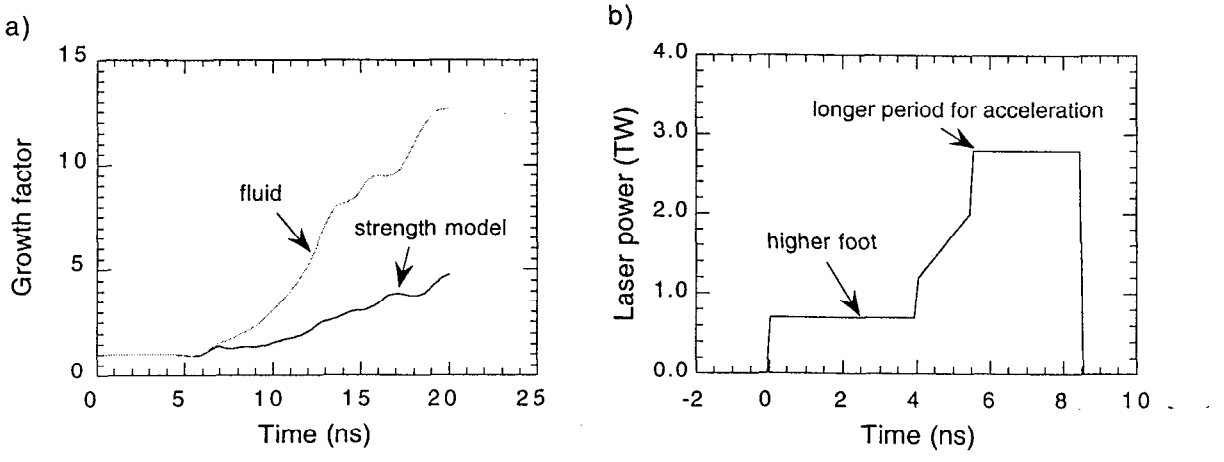

Fig. 9: a) Growth factor as a function of time calculated for a modulated Al foil with a perturbation wavelength of λ=20 μm and initial amplitude of 0.5 μm. Simulations were done with and without material strength. b) Laser pulse shape for the Al instability experiment.

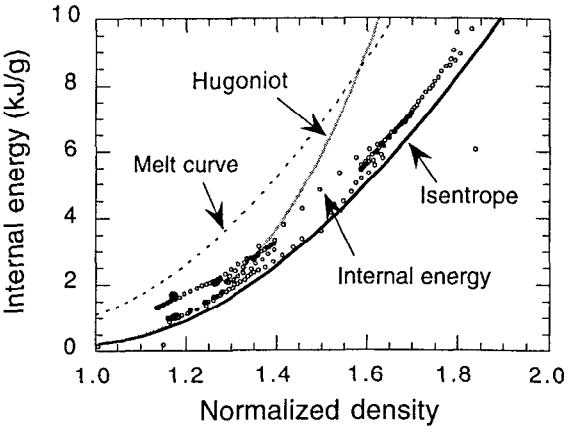

Fig. 10: Internal energy trajectory calculated for an Al foil at the CH(Br)/Al interface. The modified drive is expected to shock the foil without melting it.

SUMMARY

We have developed an x-ray drive to shock compress metal foils in the solid state using an internally shielded hohlraum with a high contrast shaped laser pulse. We use a combination of Dante measurements, side-on foil trajectories, and shock timing measurements to develop an understanding of the x-ray drive. Hydrodynamic experiments that are designed to study growth of the RT instability in the plastic flow regime have been started. Measurements of initial 20-50 μm wavelengths, and 1-2.5 μm amplitude perturbations are presented and compared with simulations in this paper. In this experiment, the growth of the instability in fluid and solid state are calculated to be nearly the same. Analytic stability analysis is consistent with the instability growing in the plastic flow regime. However, by re-designing the experiment to use an Al foil, the foil will remain in the solid state throughout, and the effect of material strength may be enhanced considerably, allowing us to conduct experiments on either side of the stability boundary.

Acknowledgement — We acknowledge the technical support of the Nova Operations and Target Fabrication groups. This work was performed under the auspices of the U.S. DOE by LLNL under contract No. W-7405-ENG-48.

REFERENCES

1. D. J. Steinberg, S. G. Cochran, M. W. Guinan, J. Appl. Phys. **51**, 1498 (1980).
2. L. C. Chhabildas, J. R. Asay, J. Appl. Phys. **50**, 2749 (1979).
3. A. I. Lebedev, P. N. Nizovtsev, V. A. Rayevsky, in the Proceedings of the 4th International Workshop on the Physics of Compressible Turbulent Mixing, 29 March - 1 April, Cambridge, England (Cambridge University Press, 1993), p. 81.
4. A. I. Lebedev, P. N. Nizovtsev, V. A. Rayevsky, V. P. Soloviov, in the Proceedings of the 6th International Workshop on the Physics of Compressible Turbulent Mixing, 17-21 June, 1997, Marseille, France (I.U.S.T.I./C.N.R.S., Marseille, 1997).
5. J. F. Barnes, P. J. Blewett, R. G. McQueen, K. A. Meyer, D. Venable, J. Appl. Phys. **45**, 727 (1974).
6. E. M. Campbell, J. T. Hunt, E. S. Bliss, D. R. Speck, R. P. Drake, Rev. Sci. Instrum. **57**, 2101 (1986).
7. P. M. Bell, J. D. Kilkenny, G. Power, R. Bonner, D. K. Bradley, in Ultrahigh Speed and High Speed Photography, Photonics, and Videography '89 (SPIE, Bellingham, WA, 1989), Proc. SPIE Vol. 1155, pp. 430-444.
8. H. N. Kornblum, R. L. Kauffman, J.A. Smith, Rev. Sci. Instrum. **57**, 2179 (1986).

9. R. L. Kauffman, H. N. Kornblum, D. W. Phillion, C. B. Darrow, B. F. Lasinski, L. J. Suter, A. R. Theissen, R. J. Wallace, F. Ze, Rev. Sci. Instrum **66**, 678 (1995).
10. G. B. Zimmerman, W. L. Kruer, Comments Plasma Phys. Controlled Fusion **2**, 51 (1975).
11. J. Lindl, Phys. Plasmas **2**, 3933 (1995).
12. K. S. Budil, P. Celliers, G. W. Collins, L. B. DaSilva, R. Cauble, R. J. Wallace, G. Chiu, A. Ng, in the Inertial Confinement Fusion Quarterly Report **7** (1), UCRL-LR-105821-97-1, 11 (1997), copies available from the National Technical Information Service, Springfield VA.
13. G. W. Collins, P. Celliers, L. B. Da Silva, R. Cauble, D. Gold, M. Foord, K. S. Budil, R. Stewart, N. C. Holmes, M. Ross, B. A. Hammel, J. D. Kilkenny, R. J. Wallace, A. Ng, Phys. Plasmas **5**, 1864 (1998).
14. Q. Johnson, A. Mitchell, R. N. Keeler, L. Evans, Phys. Rev. Lett. **25**, 1099 (1970).
15. J. S. Wark, *et al*, Phys. Rev. B **35**
16. D. H. Kalantar, *et al*, to appear in Rev. Sci. Instrum.
17. K. S. Budil, *et al*, Rev. Sci. Instrum. **67**, 485 (1996).
18. J. W. Miles, Technical Report No. GAMD-7335 (General Dynamics, San Diego, 1966).
19. D. C. Drucker, Ingenieur-Archiv **49**, 361 (1980).